Nonhomogeneous Stochastic Geometry Analysis of Massive LEO Communication Constellations

Niloofar Okati and Taneli Riihonen, *Member, IEEE*

***Abstract*— Providing truly ubiquitous connectivity requires development of low Earth orbit (LEO) satellite Internet, whose theoretical study is lagging behind network-specific simulations. In this paper, we derive analytical expressions for the downlink coverage probability and average data rate of a massive inclined LEO constellation in terms of total interference power's Laplace transform in the presence of fading and shadowing, ergo presenting a stochastic geometry-based analysis. We assume the desired link to experience Nakagami-m fading, which serves to represent different fading scenarios by varying integer m, while the interfering channels can follow any fading model without an effect on analytical tractability. To take into account the inherent non-uniform distribution of satellites across different latitudes, we model the LEO network as a nonhomogeneous Poisson point process with its intensity being a function of satellites' actual distribution in terms of constellation size, the altitude of the constellation, and the inclination of orbital planes. From the numerical results, we observe optimum points for both the constellation altitude and the number of orthogonal frequency channels; interestingly, the optimum user's latitude is greater than the inclination angle due to the presence of fewer interfering satellites. Overall, the presented study facilitates general stochastic evaluation and planning of satellite Internet constellations without specific orbital simulations or tracking data on satellites' exact positions in space.**

***Index Terms*— Massive communication satellite networks, low Earth orbit (LEO) internet constellations, interference, coverage probability, average achievable data rate, stochastic geometry, Poisson point process.**

I. Introduction

RECENT advances towards 6th generation (6G) wireless networks require progression and development of non-terrestrial networks to provide seamless connections with high transmission capacity [1]–[4]. Among non-terrestrial networks, low Earth orbit (LEO) satellite Internet constellations have gained increasing popularity as they provide global connectivity for unserved or underserved regions, where the deployment of terrestrial networks is not feasible or economically reasonable [5], [6]. Deploying thousands of satellites will ensure that every single person or appliance on Earth could be connected and no location is left in outage.

Manuscript received June 2, 2021; revised October 21, 2021 and December 22, 2021; accepted January 3, 2022. Date of publication January 14, 2022; date of current version March 17, 2022. The work of authors was supported by a Nokia University Donation. The associate editor coordinating the review of this article and approving it for publication was N. Lee. *(Corresponding author: Niloofar Okati.)*

The authors are with the Faculty of Information Technology and Communication Sciences, Unit of Electrical Engineering, Tampere University, 33720 Tampere, Finland (e-mail: niloofar.okati@tuni.fi; taneli.riihonen@tuni.fi).

Color versions of one or more figures in this article are available at https://doi.org/10.1109/TCOMM.2022.3143131.

Digital Object Identifier 10.1109/TCOMM.2022.3143131

While the performance of many LEO constellations (e.g., Starlink, OneWeb, Kuiper) has been evaluated through network-specific simulations to put the commercial plans forward, a general scientific understanding of their performance is limited in the open literature. Conventional simulation-based studies are restricted to few number of satellites with deterministic locations which is not capable of evaluating the general performance of a massive satellite network consisting of thousands of satellites. Moreover, in most of the literature, the coverage regions are assumed to have fixed circular footprints, while selecting smaller inclination angles and simultaneous consolidated operation of several LEO networks render a not-so-regular Voronoi tessellation.

In this paper, downlink coverage probability and average data rate of inclined LEO constellations are analyzed under general shadowing and fading propagation models. The satellites' positions are assumed to be distributed as a nonhomogeneous Poisson point process (NPPP), which models the satellites distribution across varying latitudes precisely by setting the intensity function to be the actual density of satellites in an actual constellation.

A. Related Works

The literature around LEO networks is mostly limited to deterministic and simulation-based analyses. In [7], the performance of two different LEO constellations was simulated assuming specific constellation sizes. The probability of average call drop and the distribution of the number of handoffs were studied for the Iridium constellation in [8]. A deterministic model to characterize the visibility time of one LEO satellite was presented in [9]. Since the model in [9] is not valid for any arbitrarily located user, authors in [10] contributed statistical analysis of coverage time in a mobile LEO constellation. In [11], a LEO-based Internet-of-Things architecture was presented so as to supply network access for devices distributed in remote areas.

Stochastic geometry is an area of mathematics, which deals with the study of random objects on Euclidean space. In the area of telecommunication, stochastic geometry has been extensively utilized to model, evaluate, and develop the wireless communication networks with irregular topologies [12]–[14], especially for two-dimensional (planar) terrestrial networks [12]–[20]. Various studies in stochastic geometry modeling of multi-tier and cognitive networks were reviewed in [15]. Observations in [16] have shown that the Poisson point process (PPP) and a regular grid model provide

lower and upper bounds on the network performance metrics, respectively, with the same deviation from the actual network performance. The research in [17] and [18], being an extension to [16], modeled a multi-tier network considering the limitations for the achievable quality-of-service. The coverage of uplink was studied in [19] assuming base stations and devices are distributed as independent PPPs.

The application of stochastic geometry to three-dimensional wireless networks has gained remarkable attention in the literature [21], [22]. In [21], a PPP model was applied to model and analyze the coverage in three-dimensional cellular networks. Since the PPP, despite providing tractable analysis, is not accurate when applied to networks with limited nodes in a finite area [23], a binomial point process (BPP) can be utilized instead to capture the characteristics of such networks [24], [25]. A finite network of unmanned aerial vehicles was modeled as a BPP in [22] and [26]. In [24] and [27], a planar network with an arbitrary shape was studied assuming the transmitter is positioned at a fixed distance. The results were then generalized in [20], by using two protocols for selecting the transmitter.

On the literature around the LEO satellite networks, the analysis is limited to few number of satellites with known locations and/or coverage spots. In [28], with tools from stochastic geometry, authors have developed a method to characterize the magnitude of Doppler shifts in a LEO network. Resource control of a satellite–terrestrial network was investigated in [29], in order to minimize the outage probability and maximize the data rate. Focusing on only a single spotbeam, the hybrid satellite–terrestrial network supporting 5G infrastructure has been presented in [30] and [31]. In [32], the outage probability of a satellite-based Internet-of-Things, in which LEO satellites relay uplink data to ground stations, is derived in closed form by assuming a low number of satellites at deterministic locations.

Recently, more research on LEO networks using stochastic geometry has started emerging. The generic coverage and rate analysis of satellite networking have been formulated in our study [33], by modeling the satellites as a BPP on a spherical shell and using the tools from stochastic geometry, without considering any deterministic model of orbits. However, the approach used in [33] is unable to include the varying density of satellites over different latitudes, except through numerical computations, to adjust the performance deviation in the actual and the uniformly modeled constellations. In fact, in practical constellations, the satellites are not evenly distributed across different latitudes [34], i.e., as the user gets farther from the equator towards the poles, more satellites are visible to it. In [34], we derived a mathematical expression, named as effective number of satellites, based on the actual constellation geometry to compensate for the performance mismatch caused by non-uniform distribution of satellites on the orbital shell.

The satellites' positions are modeled as a nonhomogeneous Poisson point process (NPPP) in [35] to analyze the coverage and rate of a noise-limited *interference-free* LEO network. Utilizing NPPP not only enables us to tractably analyze the LEO network performance, but also models the actual distribution of satellites precisely by setting its intensity to be the physical density of satellites along different latitudes. Similar contributions on performance evaluation of a LEO network were also presented in [36] using a homogeneous PPP without considering the varying density of satellites on different latitudes. The results were then used in [37] to optimize the constellation altitude.

The work in [38] characterizes the distance distribution in two different communication links in a LEO satellite network: link between a user on Earth and the nearest satellite to it and the link between a satellite and its nearest neighboring satellite. Unlike in [33], the satellites are assumed to be placed at different known altitudes, i.e., on multiple orbital shells. Stochastic geometry and the results from [38] were then utilized in [39] to obtain the downlink probability of coverage for a LEO network, where satellite gateways act as relays between the satellites and users on Earth. An uplink communication scenario was characterized by considering interfering terrestrial transmitters in [40].

This paper, unlike our prior works [33], [34], adopts nonhomogeneous Poisson point process to model the satellites' locality, for which the varying density along different latitudes is embedded in the PPP's intensity function. Moreover, a more general fading model, i.e., Nakagami-m, transceivers' antenna patterns, and shadowing attenuation due to the blockage of the signals by obstacles surrounding the user, are considered in our analysis. This paper also includes interference analysis in a generic form which was neglected in [35] and the performance metrics are evaluated in terms of the Laplace function of interference.

B. Contributions and Paper Organization

We model the satellites' positions in a LEO network as a nonhomogeneous PPP which facilitates not only using the tools from stochastic geometry, but also capturing the exact characteristics of the actual constellations, i.e., the uneven distribution of satellites across different latitudes. Unlike in [33], [34], and [39], by selecting the intensity of NPPP to fit the actual distribution of satellites on an orbital shell, there is no mismatch between the performance of theoretical stochastic constellations and actual deterministic LEO networks. We derive the intensity of NPPP in closed form in terms of the constellation parameters: the total number of satellites, altitude of the constellation, latitude of the satellites, and the inclination of the orbits. The model is extensible to develop an analysis on satellite-to-satellite communication, similar to what was proposed in [41] for three-dimensional wireless sensor networks.

As the main contributions, we utilize stochastic geometry to formulate the coverage and average achievable rate of a user served by a LEO constellation in terms of the derivative of Laplace transform of interference power.[1] Our derivations do not rely on exact location of every single satellite and are applicable for performance analysis of any given constellation

[1]Thus, the present study, unlike the preliminary results presented in [35] that are limited to the special case of scheduling an orthogonal channel for every satellite, includes the cumulative interference from all other satellites that are visible to the user and share the same channel.

as long as the constellation parameters are known. Modeling the satellites' locality as a NPPP, the analytical expressions obtained from a stochastic constellation geometry can be particularly used to analyze the actual deterministic constellations.

In propagation modelling, unlike most of literature on this topic, we take into account the effect of shadowing caused by the presence of the obstacles surrounding the user. To retain analytical tractability and still cover different fading scenarios, we assume Nakagami-m fading with integer m as well as shadowing with any desired distribution for the propagation model of desired links.[2] For interfering signals, any arbitrarily distributed fading and shadowing can be considered, since the analytical tractability is unaffected. Frequency reuse has been also taken into account by randomly assigning the frequency channels to the satellites. Random channel assignment preserves the tractability of our analytical derivations since it can be modeled by thinning the original nonhomogeneous Poisson point process.

In this paper, antenna pattern, despite the conventional approach, is formulated and included in the performance analysis by representing the antenna gain as a function of the relative distances between the user and the satellites. Finally, we evaluate two critical performance metrics, i.e., coverage and data rate, in terms of several key design parameters, such as altitude of the constellation and the number of frequency channels. From the numerical results, we are able to observe optimal points for these parameters for some specific network setup. Counter-intuitively, the user which resides in higher latitudes, away from the constellation borders, has the best performance due to existence of fewer interfering satellites in that region. Some constellation design guidelines, e.g., on orbital inclination and altitude, are also provided through the numerical results.

The remainder of this paper is organized as follows. Section II describes the system model and the mathematical preliminaries for modeling a LEO network as a NPPP. The main outcome of this study, which is the derivation of analytical expressions for downlink coverage probability and average achievable rate of a terrestrial user, is presented in Section III, which involves also the analysis of the Laplace transform of interference power. We provide numerical results in Section IV for the verification of our derivations and studying the effect of key system parameters such as the size of the constellation and its altitude as well as the channel parameters on the network performance. Finally, we conclude the paper in Section V.

II. System Model

In this section, first, we present the characteristics and geometries of actual low Earth orbit satellite constellations. Next, we will introduce the mathematical preliminaries for modeling the actual network as a stochastic point process.

A. Actual Inclined Constellations

As shown in Fig. 1, we consider a LEO communication satellite constellation consisting of N satellites launched uniformly on circular orbits with inclination angle, ι, and altitude that is denoted by $r_{\min}$ — the subscript indicates the minimum possible distance between a satellite and a ground user (as measured at the zenith). Satellites' spherical coordinates in terms of their latitude and longitude are denoted by $(\phi_{\rm s}, \lambda_{\rm s})$.

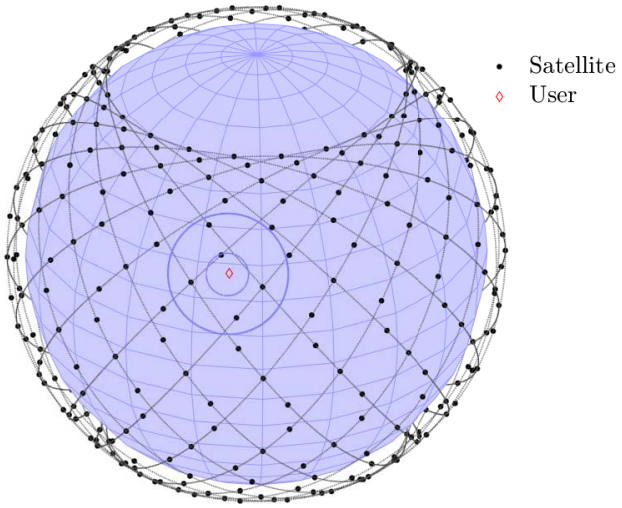

Fig. 1. A constellation in an example case of $N = 400$ satellites flying on $\iota = 53^\circ$ inclined orbits. The borders of two spherical caps above the user are shown: the outer one covers all visible satellites to the user while the inner one is empty of satellites and the serving satellite is located on its border.

A user terminal is located on any specific latitude, denoted by $\phi_{\rm u}$, on the surface of Earth that is approximated as a perfect sphere with radius $r_\oplus \approx 6371$ km. Satellites rising above the horizon at an angle of $\theta_{\rm s} \geq \theta_{\min}$ are the only ones capable of transmitting signals to the users. As such, $r_{\max}$ refers to the maximum distance at which a satellite and a user are able to communicate (and it occurs when $\theta_{\rm s} = \theta_{\min}$), and

$$\frac{r_{\max}}{r_\oplus} = \sqrt{\frac{r_{\min}}{r_\oplus}\left(\frac{r_{\min}}{r_\oplus} + 2\right) + \sin^2(\theta_{\min})} - \sin(\theta_{\min}). \quad (1)$$

In this paper, the serving satellite is the one with the shortest distance to the user. We perform frequency reuse by assuming K, with $K \leq N$, orthogonal frequency channels available for the network. The satellites are distributed randomly among the channels, which potentially causes co-channel interference to the user from $\frac{N}{K} - 1$ satellites which share the same frequency channel. All satellites on the same channel that are elevated above the horizon to an angle of $\theta_{\rm s} \geq \theta_{\min}$ cause interference to reception of the user.

The variables R_0 and R_n, $n = 1, 2, \ldots, N$, represent the distances from the user to the serving satellite and the other interfering satellites, respectively, while H_0 and H_n denote the corresponding channel gains to model fading. Shadowing effect is modeled by random variables $\mathcal{X}_n$, $n = 1, 2, \ldots, N$, correspondingly. It is worth noting that losses caused by near-ground obstacles in the last few meters of the signal path, named as excess path loss in [36], can be approximated by properly setting the shadowing distribution and its corresponding parameters. On the other hand, our analysis

[2]Varying the value of m, we are able to control the multi-path fading severity. For instance, $m = 1$ corresponds to Rayleigh fading environment while $m \to \infty$ represents non-fading channels.

is also capable of including the effect of elevation angle on the shadowing by expressing it as a function of the relative distances between the user and the satellites. However, in this paper, we do not explicitly formulate that to simplify the expressions. Obviously, $H_n = \mathcal{X}_n = 0$ if $R_n > r_{\max}$ for some $n = 0, 1, \ldots, N$. The attenuation due to atmospheric gases is insignificant for frequencies below 20 GHz (at least, or even at higher bands below the oxygen absorption peak at 60 GHz) [42, Fig. 10], which is the practical range for downlink LEO communication in well-known constellations [43].

For the serving channel, we adopt Nakagami-m fading which will enable not only to consider a wide range of multi-path fading conditions but also to maintain the tractability of our derivations. On the other hand, for the interfering channels, we consider arbitrary fading distributions since they have no effect on the tractability of our analysis and, hence there is no need to limit our results to some specific fading models. Following the same logic, we also obtain more general results by assuming arbitrarily distributed shadowing for all — the serving and the interfering — channels.

To simplify notation, when $N_{\rm I} > 0$, we let indices $n = 1, 2, \ldots, N_{\rm I}$ correspond to those $N_{\rm I} \leq N/K - 1$ satellites with $\theta_{\rm s} \geq \theta_{\min}$ that cause co-channel interference. The user and the satellites are equipped with directional antennas having gains denoted by $G_{\rm u}(\theta_{\rm u})$ and $G_{\rm s}(\theta_n)$, respectively, while $\theta_{\rm u}$ and θ_n are the angles between the line-of-sight path and their corresponding antennas' boresight. We assume that the user's antenna boresight is directed towards the sky, perpendicular to Earth's surface, and the satellites' antennas' boresight always radiates towards the center of Earth. When all antennas have symmetrical radiation patterns, using the law of cosines, we obtain $\theta_{\rm u}$ and θ_n as

$$\theta_{\rm u}(R_n) = \pi - \cos^{-1}\left(\frac{r_\oplus^2 + R_n^2 - (r_\oplus + r_{\min})^2}{2 r_\oplus R_n}\right) \tag{2}$$

and

$$\theta_n(R_n) = \cos^{-1}\left(\frac{R_n^2 - r_\oplus^2 + (r_\oplus + r_{\min})^2}{2R_n\,(r_\oplus + r_{\min})}\right), \tag{3}$$

respectively. As can be seen from (2) and (3), the antennas' radiation patterns are one-to-one functions of the relative distances between the user and the satellites. Thus, in the rest of this paper, we will denote the user's and the satellites' antenna gains directly as $G_{\rm u}(R_n)$ and $G_{\rm s}(R_n)$, respectively, and $G_{\rm t}(R_n) = G_{\rm u}(R_n)G_{\rm s}(R_n)$ is the overall antenna gain.

According to the described model, the signal-to-interference-plus-noise ratio (SINR) of the link is given by

$$\mathrm{SINR} = \frac{p_{\rm t} G_{\rm t}(R_0) H_0 \mathcal{X}_0 R_0^{-\alpha}}{I + \sigma^2}, \tag{4}$$

where $p_{\rm t}$ is the transmit power of satellites, the constant σ^2 is the additive noise power, the parameter α is a path loss exponent, which should be set to $\alpha = 2$ for satellite communication since the signal travels through free space for most of its path, and

$$I \triangleq \sum_{n=1}^{N_{\rm I}} p_{\rm t} G_{\rm t}(R_n) H_n \mathcal{X}_n R_n^{-\alpha} \tag{5}$$

is the cumulative interference power from all $N_{\rm I}$ other satellites above the user's horizon that share the same frequency channel with the serving satellite. The distance from the user to its nearest satellite is

$$R_0 = \min_{n=1,2,\ldots,N_{\rm vis}} R_n, \tag{6}$$

where $N_{\rm vis}$ is a variable representing the number of visible satellites to the user (cf. the outer cap in Fig. 1).

B. Nonhomogeneous PPP Model

In the constellation described earlier, the satellites appear unevenly along the lines of latitudes, which means, e.g., that there are more visible satellites for a user located close to inclination limits than for one on equatorial region. In order to model the latitude-dependent distribution of satellites, we assume that the satellites are distributed according to a *nonhomogeneous* PPP, ξ, on a spherical surface with radius $r_\oplus + r_{\min}$. The NPPP is characterized with its intensity, $\delta(\phi_{\rm s}, \lambda_{\rm s})$, which varies according to the satellites' latitude (and/or longitude).

By the definition of a NPPP, the number of points in some bounded region $\mathcal{A}$ of the orbital shell is a Poisson-distributed random variable denoted by $\mathcal{N}$. Thereby, the probability to have n satellites in $\mathcal{A}$ is given by

$$\begin{aligned} P_n(\mathcal{A}) &\triangleq \mathbb{P}(\mathcal{N} = n) \\ &= \frac{1}{n!}\left(\iint_{\mathcal{A}} \delta(\phi_{\rm s}, \lambda_{\rm s})\,(r_{\min} + r_\oplus)^2 \cos(\phi_{\rm s})\, d\phi_{\rm s} d\lambda_{\rm s}\right)^n \\ &\quad \times \exp\left(-\iint_{\mathcal{A}} \delta(\phi_{\rm s}, \lambda_{\rm s})\,(r_{\min} + r_\oplus)^2 \cos(\phi_{\rm s})\, d\phi_{\rm s} d\lambda_{\rm s}\right), \end{aligned} \tag{7}$$

where $\delta(\phi_{\rm s}, \lambda_{\rm s})$ is the intensity function of nonhomogeneous PPP at latitude $\phi_{\rm s}$ and longitude $\lambda_{\rm s}$. Based on the given system model, $\mathcal{A}$ is the spherical cap where viewable satellites to the user exist (cf. the outer one in Fig. 1), with surface area $\left(\delta\pi\left(r_{\max}^2 - r_0^2\right)\right)/(1 - \frac{r_{\min}}{r_\oplus + r_{\min}})$ (See [33, Appendix A]).

In order to precisely model a LEO network as a NPPP, we first need to characterize the intensity function based on the actual physical network as follows. The preliminaries obtained herein will be used shortly towards contributing expressions for probability of coverage and average achievable rate.

Lemma 1: When satellites are distributed uniformly on low circular orbits with the altitude, $r_{\min}$, and the inclination angle, ι, the intensity function of the nonhomogeneous PPP is a function of latitude, $\phi_{\rm s}$, only and given by

$$\delta(\phi_{\rm s}) = \frac{N}{\sqrt{2}\pi^2 (r_{\min} + r_\oplus)^2} \cdot \frac{1}{\sqrt{\cos(2\phi_{\rm s}) - \cos(2\iota)}}, \tag{8}$$

and we can denote $\delta(\phi_{\rm s}, \lambda_{\rm s}) = \delta(\phi_{\rm s})$ since it does not depend on $\lambda_{\rm s}$, for $\phi_{\rm s} \in [-\iota, \iota]$.

Proof: The intensity function is equivalent to the actual density of the satellites on an orbital shell element created by

TABLE I
SUMMARY OF MATHEMATICAL NOTATION

Notation	Description
$r_\oplus; r_{\min}; r_{\max}$	Earth radius (6371 km); Constellation altitude; Maximum possible distance between a user and a visible satellite
$R_0;\ R_n$	Serving distance; Distance to the n^{th} satellite
$N; N_{\text{I}}; K$	Constellation size; The number of interfering satellites; The number of frequency channels
$G_{\text{u}}; G_{\text{s}}; G_{\text{t}}$	Antenna gain of the user; Antenna gain of the n^{th} satellite; Overall antenna gain
$H_0; H_n$	Channel fading gain of the serving link; Channel fading gain of the n^{th} link
$\mathcal{X}_0; \mathcal{X}_n$	Shadowing component of the serving link; Shadowing component of the n^{th} link
α	Path loss exponent
p_{t}	Transmission power satellites
σ^2	Additive noise power
T	SINR threshold for coverage probability
$P_{\text{c}}; C$	Coverage probability; Average achievable rate

spanning the azimuthal angle from 0° to 360° on the orbital shell at latitude ϕ_{s}, that is calculated as

$$\delta(\phi_{\text{s}}) = \frac{N f_{\Phi_{\text{s}}}(\phi_{\text{s}})\, d\phi_{\text{s}}}{2\pi(r_{\min}+r_\oplus)^2 \cos(\phi_{\text{s}})\, d\phi_{\text{s}}}, \tag{9}$$

which is the ratio of the number of satellites resided on the surface element to the element's area. Substituting the probability density $f_{\Phi_{\text{s}}}(\phi_{\text{s}})$ of random latitude Φ_{s} [34, Lemma 2] completes the proof. □

If the intensity of satellites is simplistically presumed to be uniform all over the orbital shell, it can be written as follows.

Lemma 2: When satellites are uniformly distributed on a sphere, the point process turns into a homogeneous Poisson point process with a constant intensity given by

$$\delta = \frac{N}{4\pi(r_{\min}+r_\oplus)^2}, \tag{10}$$

which does not depend on latitudinal/longitudinal parameters.

Thus, for the special case when satellites are distributed uniformly on the orbital shell, by substitution from Lemma 2, the probability given in (7) can be expressed in closed form as

$$P_n(\mathcal{A}) = \frac{1}{n!}\left(\frac{N\left(r_{\max}^2 - r_{\min}^2\right)}{4r_\oplus\left(r_\oplus + r_{\min}\right)}\right)^n \exp\left(-\frac{N\left(r_{\max}^2 - r_{\min}^2\right)}{4r_\oplus\left(r_\oplus + r_{\min}\right)}\right). \tag{11}$$

III. PERFORMANCE ANALYSIS

In this section, we focus on the performance analysis of a LEO satellite network in terms of coverage probability and data rate of a user in an arbitrary location on Earth. We utilize stochastic geometry in order to formulate coverage probability and rate as a function of the network and the propagation parameters. Two main components of our analytical derivations are the distribution of the distance to the nearest satellite and the Laplace function of interference which will be presented throughout this section.

A. The Distance to the Nearest Satellite

In this paper, the serving satellite is assumed to be the nearest one to the user. Therefore, an important parameter for coverage and rate analysis is the probability density function (PDF) of the distance to the nearest satellite, R_0, which is given as follows.

Lemma 3: The PDF of the serving distance R_0, when the satellites are distributed according to a nonhomogeneous PPP with a latitude-dependent intensity, $\delta(\phi_{\text{s}})$, is

$$f_{R_0}(r_0) = 2r_0\left(\frac{r_{\min}}{r_\oplus}+1\right)\exp(-\gamma(r_0))\int_{\max(\phi_{\text{u}}-\phi_0,-\iota)}^{\min(\phi_{\text{u}}+\phi_0,\iota)} \delta(\phi_{\text{s}}) \times \frac{\cos(\phi_{\text{s}})}{\sqrt{\cos^2(\phi_{\text{s}}-\phi_{\text{u}}) - \cos^2(\phi_0)}} d\phi_{\text{s}}, \tag{12}$$

where

$$\gamma(r_0) = 2(r_{\min}+r_\oplus)^2 \times \int_{\max(\phi_{\text{u}}-\phi_0,-\iota)}^{\min(\phi_{\text{u}}+\phi_0,\iota)} \delta(\phi_{\text{s}})\cos(\phi_{\text{s}})\cos^{-1}\left(\frac{\cos(\phi_0)}{\cos(\phi_{\text{s}}-\phi_{\text{u}})}\right) d\phi_{\text{s}} \tag{13}$$

and ϕ_0 is the polar angle difference between the serving satellite and the user which is given by $\phi_0 = \cos^{-1}\left(1 - \frac{r_0^2 - r_{\min}^2}{2(r_{\min}+r_\oplus)r_\oplus}\right)$. Equation (12) is valid for $\phi_0 \geq |\phi_{\text{u}}| - \iota$ and $r_0 \in [r_{\min}, 2r_\oplus + r_{\min}]$ while $f_{R_0}(r_0) = 0$ otherwise.

Proof: See Appendix A. □

We validate the PDF of the serving distance given in Lemma 3 (lines) by Monte Carlo simulations (markers) in Fig. 2. As shown in the figure, for larger number of satellites, it is more likely that the serving distance has a value close to the constellation altitude. The PDF becomes more uniform and its maximum point diverges from the constellation altitude for fewer number of satellites. For user's latitudes greater than the inclination angle, e.g., $\phi_{\text{u}} = 65^\circ$ in the figure, the serving distance has a value greater than the altitude depending the constellation size and its altitude.

When the density of satellites is presumed to be uniform, i.e., it is not a function of latitude, the PDF of the serving distance can be obtained in closed form as follows.

Lemma 4: The PDF of the serving distance R_0 when the satellites are distributed uniformly with constant intensity given in Lemma 2 is

$$f_{R_0}(r_0) = \frac{N r_0}{2r_\oplus(r_{\min}+r_\oplus)} \exp\left(-N\left(\frac{r_0^2 - r_{\min}^2}{4(r_{\min}+r_\oplus)r_\oplus}\right)\right) \tag{14}$$

for $r_0 \in [r_{\min}, 2r_\oplus + r_{\min}]$ while $f_{R_0}(r_0) = 0$ otherwise.

Proof: In this proof, the same principles are used as in Lemma 3. However, the integration from a constant density

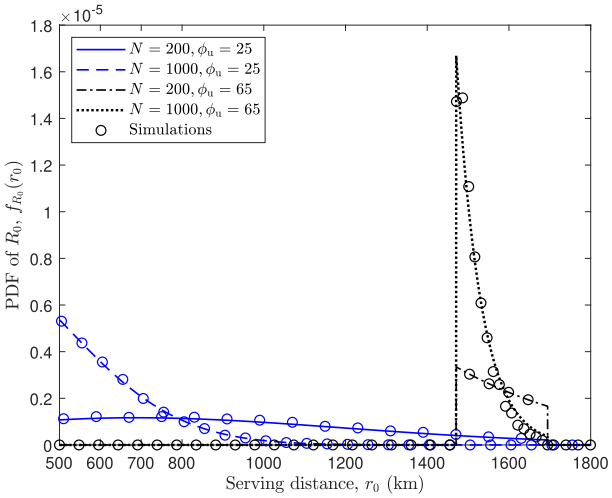

Fig. 2. PDF of the serving distance, R_0, given in Lemma 3, for $r_{\min} = 500$ km, $\iota = 53°$, and $\theta_{\min} = 10°$. The lines and the markers show the theoretical and simulation results, respectively.

over the cap sphere will reduce to a simple expression. Thus, $F_{R_0}(r_0) = 1 - \exp\left(-N\left(\frac{r_0^2 - r_{\min}^2}{4(r_{\min}+r_\oplus)r_\oplus}\right)\right)$. Calculating the derivative of the CDF w.r.t. r_0 completes the proof. □

The PDF of the serving distance is also derived in [33] assuming satellites are uniformly distributed as a BPP. It is worth noting that the Taylor series expansion of Lemma 4 and the serving distance distribution given in [33, Lemma 2] are the same for the first two terms. The difference between the serving distance in a uniformly distributed constellation given in [33] and the homogeneous Poisson point process in Lemma 4 is insignificant since the argument of exponential function in (14), i.e., $N\left(\frac{r_0^2 - r_{\min}^2}{4(r_{\min}+r_\oplus)r_\oplus}\right)$, is small.

B. Coverage Probability and Average Data Rate

The coverage probability is the probability that the SINR at the receiver is higher than the minimum SINR required to successfully transmit the data. The coverage probability is defined as

$$P_{\rm c}(T) \triangleq \mathbb{P}(\text{SINR} > T) = \mathbb{P}\left(\frac{p_{\rm t} G_{\rm t}(R_0) H_0 \mathcal{X}_0 R_0^{-\alpha}}{I + \sigma^2} > T\right), \tag{15}$$

where T is the SINR threshold.

Using the above definition, we express the coverage probability of a user in the following theorem.

Theorem 1: The coverage probability for an arbitrarily located user under a Nakagami fading serving channel while both shape parameter and rate parameter of gamma distribution[3] are m_0, is

$$P_{\rm c}(T) \triangleq \mathbb{P}(\text{SINR} > T) = \int_{r_{\min}}^{r_{\max}} \int_0^\infty f_{\mathcal{X}_0}(x_0) f_{R_0}(r_0) \left[e^{-s\sigma^2} \sum_{k=0}^{m_0-1} \frac{\sum_{l=0}^{k} \binom{k}{l} (s\sigma^2)^l (-s)^{k-l} \frac{\partial^{k-l}}{\partial s^{k-l}} \mathcal{L}_I(s)}{k!} \right]_{s=\frac{m_0 T r_0^\alpha}{p_{\rm t} G_{\rm t}(r_0) x_0}} dx_0 dr_0, \tag{16}$$

[3]Channel gain, being the square of Nakagami random variable, follows a gamma distribution.

where the PDF $f_{R_0}(r_0)$ is given in Lemma 3 (or Lemma 4), $f_{\mathcal{X}_0}(x_0)$ is the PDF of $\mathcal{X}_0$ and $\mathcal{L}_I(s)$ is the Laplace transform of interference power I calculated in the next section.

Proof: See Appendix B. □

Let us then move on the average achievable data rate (in bit/s/Hz), which is the ergodic capacity for a fading communication link derived from Shannon-Hartley theorem normalized to unit bandwidth. The average achievable rate is defined as

$$\bar{C} \triangleq \frac{1}{K} \mathbb{E}\left[\log_2(1 + \text{SINR})\right]. \tag{17}$$

Unlike for the coverage probability, frequency reuse affects the average rate in two opposite directions. One direction is the improvement in SINR due to the reduction in the number of interfering satellites which use the same channel. The other direction which results in lower data rate is induced by a reduction in the availability of the frequency band shared among a group of satellites.

In the following theorem, we calculate the expression for the average rate of a user over Nakagami fading serving channel. The interfering channel gains may follow any arbitrary distribution.

Theorem 2: The average data rate of an arbitrarily located user under a Nakagami fading serving channel and any fading or shadowing distribution for interfering channels is given by

$$\bar{C} = \frac{1}{K} \int_{r_{\min}}^{r_{\max}} \int_0^\infty \int_0^\infty f_{\mathcal{X}_0}(x_0) f_{R_0}(r_0) \left[e^{-s\sigma^2} \sum_{k=0}^{m_0-1} \frac{\sum_{l=0}^{k} \binom{k}{l} (s\sigma^2)^l (-s)^{k-l} \frac{\partial^{k-l}}{\partial s^{k-l}} \mathcal{L}_I(s)}{k!} \right]_{s=\frac{m_0(2^t-1) r_0^\alpha}{p_{\rm t} G_{\rm t}(r_0) x_0}} dt dx_0 dr_0, \tag{18}$$

where m_0 is the parameter of Nakagami fading, and $\mathcal{L}_I(s)$ will be given in Lemma 5 and its corresponding corollaries, which cover some special cases.

Proof: See Appendix C. □

C. Interference Analysis

In this subsection, we derive the Laplace function of interference which is a key element of the performance expressions in Theorems 1 and 2. We, first, obtain the expression considering a general propagation model which means that no assumption is made regarding the specific expressions of $f_{\mathcal{X}_n}(x_n)$ and $f_{H_n}(h_n)$.

Lemma 5: When the server is at distance $r_0 \geq r_{\min}$ from the user and interfering channels experience an arbitrary distributed fading, the Laplace transform of random variable I is

$$\mathcal{L}_I(s) \triangleq \mathbb{E}_I\left[e^{-sI}\right] = \sum_{n=0}^{\infty} P_n\left(\mathcal{A}(r_{\max}) - \mathcal{A}(r_0)\right) \times \left(\int_{r_0}^{r_{\max}} \int_0^\infty \mathcal{L}_{H_n}(s p_{\rm t} G_{\rm t}(r_n) x_n r_n^{-\alpha}) f_{\mathcal{X}_n}(x_n) f_{R_n|R_0}(r_n|r_0) dx_0 dr_n \right)^n, \tag{19}$$

where

$$f_{R_n|R_0}(r_n|r_0) = \frac{d\gamma(r_n)/dr_n}{\gamma(r_{\max}) - \gamma(r_0)} \tag{20}$$

is the probability density function of the distance from any visible satellite to the user conditioned on the serving distance [33, Lemma 3]. The parameter $\mathcal{A}(r_{\max})$ represents the spherical cap where all satellites that can be viewed by the user exist while $\mathcal{A}(r_0)$ is the cap above the user, empty of satellites and with the serving satellite on its border (base of the cap). The function $f_{\mathcal{X}_n}(x_n)$ denotes the shadowing PDF for the nth interfering channel.

Proof: See Appendix D. □

In the special cases, where channels experience Nakagami fading without any shadowing, Lemma 5 can be reduced into the following corollary. The expression thereof is obtained by substituting the Laplace function of a gamma random variable, i.e., $\mathcal{L}_{H_n}(z) = \frac{m_n^{m_n}}{(m_n+z)^{m_n}}$, where m_n stands for both shape parameter and rate parameter of gamma distribution for the nth link.

Corollary 1: When the interfering channels experience only Nakagami fading (no shadowing), the Laplace function of interference can be written as

$$\mathcal{L}_I(s) = \sum_{n=0}^{\infty} P_n\left(\mathcal{A}(r_{\max}) - \mathcal{A}(r_0)\right) \times \left(\int_{r_0}^{r_{\max}} \frac{m_n^{m_n}}{(m_n + sp_{\mathrm{t}}G_{\mathrm{t}}(r_n) r_n^{-\alpha})^{m_n}} f_{R_n|R_0}(r_n|r_0) dr_n \right)^n, \tag{21}$$

where $\mathcal{A}(r_{\max})$ and $\mathcal{A}(r_0)$ are the visible cap and the null cap above the user, respectively. The PDF $f_{R_n|R_0}(r_n|r_0)$ is given in (20)*, and m_n is the Nakagami fading parameter for nth link.*

When the intensity of the PPP is presumed to be constant (regardless of the latitude), the Laplace function can be obtained from the following corollary by simply substituting $\gamma(\cdot)$ in (20) by the product of the density in Lemma 2 and the surface area of the spherical cap formed by the distance between the user and the given interfering satellite.

Corollary 2: The Laplace function of interference when the satellites are distributed uniformly with constant intensity, and their channels experience Nakagami fading, is given by

$$\mathcal{L}_I(s) = \sum_{n=0}^{\infty} \frac{1}{n!} \left(\frac{N\left(r_{\max}^2 - r_0^2\right)}{4r_{\oplus}\left(r_{\oplus} + r_{\min}\right)} \right)^n \exp\left(-\frac{N\left(r_{\max}^2 - r_0^2\right)}{4r_{\oplus}\left(r_{\oplus} + r_{\min}\right)} \right) \times \left(\int_{r_0}^{r_{\max}} \int_0^{\infty} \frac{2 r_n m_n^{m_n} f_{\mathcal{X}_0}(x_0)}{\left(r_{\max}^2 - r_0^2\right)\left(m_n + sp_{\mathrm{t}}G_{\mathrm{t}}(r_n) r_n^{-\alpha}\right)^{m_n}} dx_0 dr_n \right)^n, \tag{22}$$

where $f_{\mathcal{X}_n}(x_n)$ is the PDF of the shadowing component and m_n is the fading parameter for Nakagami fading.

The following corollary presents the Laplace function of interference in closed-form, under the assumptions given in Corollary 2 and additionally excluding shadowing from the propagation model.

Corollary 3: Assuming constant antenna gains, the Laplace function of interference, when the satellites are distributed uniformly with constant intensity and their channels experience only Nakagami fading (no shadowing), is given by

$$\mathcal{L}_I(s) = \sum_{n=0}^{\infty} \frac{1}{n!} \left(\frac{N\left(r_{\max}^2 - r_0^2\right)}{4r_{\oplus}\left(r_{\oplus} + r_{\min}\right)} \right)^n \exp\left(-\frac{N\left(r_{\max}^2 - r_0^2\right)}{4r_{\oplus}\left(r_{\oplus} + r_{\min}\right)} \right) \times \frac{1}{\left(r_{\max}^2 - r_0^2\right)} \left[r_{\max}^2 \, {}_2F_1\left(-\frac{2}{\alpha}, m_n; \frac{\alpha-2}{\alpha}; -\frac{sp_{\mathrm{t}}G_{\mathrm{t}} r_{\max}^{-\alpha}}{m_n} \right)^n - r_0^2 \, {}_2F_1\left(-\frac{2}{\alpha}, m_n; \frac{\alpha-2}{\alpha}; -\frac{sp_{\mathrm{t}}G_{\mathrm{t}} r_0^{-\alpha}}{m_n} \right)^n \right], \tag{23}$$

where ${}_2F_1(\cdot,\cdot;\cdot;\cdot)$ is the Gauss's hyper-geometric function and m_n is the fading parameter.

Finally, using the function given in [44, Eq. 9.100] and substitution from special parameter values, the above can be reduced to elementary functions. For instance, when $m = 1$ and $\alpha = 2$, we have

$$\mathcal{L}_I(s) = \sum_{n=0}^{\infty} \frac{1}{n!} \left(\frac{N\left(r_{\max}^2 - r_0^2\right)}{4r_{\oplus}\left(r_{\oplus} + r_{\min}\right)} \right)^n \exp\left(-\frac{N\left(r_{\max}^2 - r_0^2\right)}{4r_{\oplus}\left(r_{\oplus} + r_{\min}\right)} \right) \times \left(1 + \frac{sp_{\mathrm{t}}G_{\mathrm{t}}}{\left(r_{\max}^2 - r_0^2\right)} \ln\left(\frac{k + r_0^2}{k + r_{\max}^2} \right) \right). \tag{24}$$

To perform frequency reuse, we assign each satellite randomly and independently to a particular frequency channel. Therefore, the satellites assigned to each of the orthogonal frequency channels form a thinned version of the original PPP with intensity $\delta(\phi_{\mathrm{s}})/K$. Since thinning preserves the Poisson point process according the thinning theorem of PPP [13], we can take into account the effect of frequency reuse by substitution $\delta(\phi_{\mathrm{s}}) \rightarrow \delta(\phi_{\mathrm{s}})/K$ in Laplace function of interference (in Lemma 5 or the corresponding corollaries). Since the same frequency channel is used by the user and its nearest satellite, the frequency reuse has no effect on the original value of intensity that is used to obtain the PDF of the distance from the user to the server in Lemma 3.

IV. Numerical Results

In this section, we provide numerical results to study the effect of different network parameters on coverage probability and average data rate using the analytical expressions obtained in Section III. The performance of the network is evaluated in terms of satellite altitude and the number of orthogonal frequency channels, which provides important guidelines into the satellite network design. Furthermore, our analytical derivations are all verified through Monte Carlo simulations.

We consider the large-scale attenuation with path loss exponent $\alpha = 2$, and the small-scale Nakagami-m fading with integer $m \in \{1, 2, 3\}$. The choice of the fading

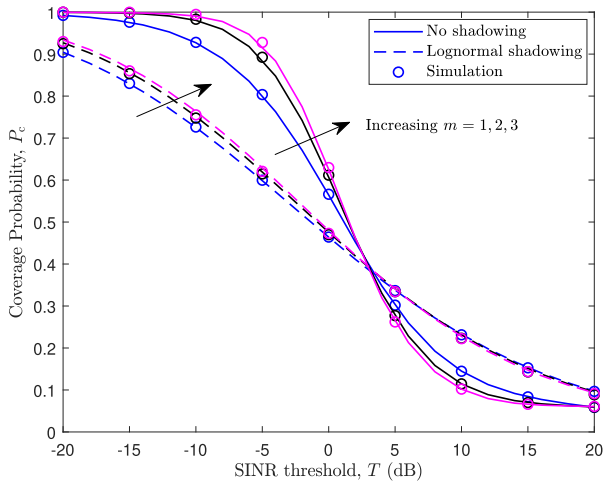

Fig. 3. Theorem 1 verification with simulations when $\phi_{\rm u} = 25°$, $\iota = 53°$, $m \in \{1, 2, 3\}$, and $\theta_{\min} = 10°$. The lines and the markers show the theoretical and simulation results, respectively.

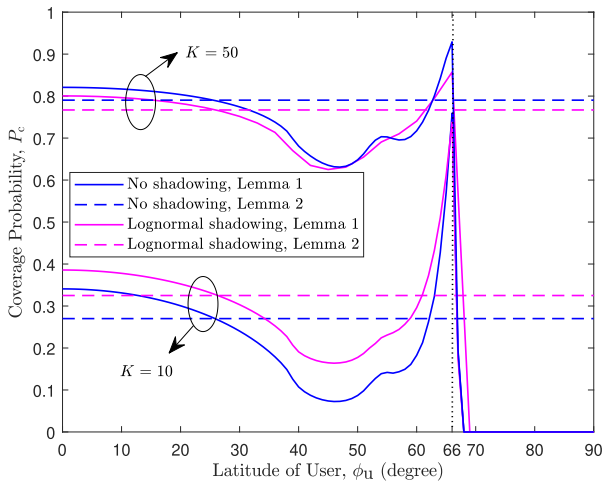

Fig. 4. Theoretical coverage probability on different users' latitudes, $T = 5$ dB, $r_{\min} = 500$ km, $\iota = 53°$, $m = 2$, and $\theta_{\min} = 10°$. The expression given in Theorem 1 is used to plot this figure.

parameter corresponds to several cases when a dominant line-of-sight component is not available for the user due to being in highly dense urban areas or at higher latitudes compared to the inclination limits. We assume lognormal shadowing which is represented as $\mathcal{X}_0 = 10^{X_0/10}$ such that X_0 has a normal distribution with mean $\mu_{\rm s} = 0$ and standard deviation $\sigma_{\rm s} = 9$ dB. Thus, the PDF of lognormal shadowing is

$$f_{\mathcal{X}_0}(x_0) = \frac{10}{\ln(10)\sqrt{2\pi}\sigma_{\rm s} x_0} \exp\left(-\frac{1}{2}\left(\frac{10\log_{10}(x_0) - \mu_{\rm s}}{\sigma_{\rm s}}\right)^2\right). \tag{25}$$

The number of orthogonal channels is set to $K = 10$ in all the numerical results unless otherwise stated. We assume ideal isotropic antennas for the satellites as well as the user. The equivalent isotropic radiated power (EIRP) and the noise power are set to 40 dBm, and -103 dBm, respectively. The operating frequency is assumed to be 2 GHz. For the reference simulations, satellites are placed uniformly on orbits centered at Earth's center with radius $r_\oplus + r_{\min}$.

Figure 3 verifies our derivations given in Theorem 1 for $53°$ inclined orbits and a user located at $25°$ latitude. The total number of satellites and constellation altitude are chosen to be 2000 and 500 km, respectively. As shown in the figure, the markers that depict the Monte Carlo simulation results are completely matched with the lines that represent our theoretical expressions. Shadowing, as a random phenomenon, may cause an increase or decrease in the received SINR at the user's place. As a result, a varying effect of shadowing on the coverage probability can be observed for different SINR threshold values in Fig. 3. Obviously, this behaviour is thoroughly affected by the mean and variance of lognormal shadowing. Larger values of m correspond to higher elevation angles and, consequently, less multi-path distortion, which result in slightly better coverage, but shadowing masks the effect of fading at large.

The effect of user's latitude on coverage probability is depicted in Fig. 4 for $K = 10$ and 50. The coverage probability when satellites form a NPPP with intensity given in Lemma 1 is shown by solid lines. Since the intensity increases as the user moves to higher latitudes, the performance becomes more unreliable due to increase in the density of satellites that share the same frequency channel with the user's serving satellite. When the user is in higher latitudes than the constellation inclination limits, the coverage probability starts increasing due to the reduction in the number of visible interferers. The coverage reaches its maximum at about $66°$ where the serving satellite is the only visible satellite to the user, i.e., the performance becomes noise-limited. For latitudes larger than $66°$, the coverage converges to zero quickly, since there are no satellites above horizon to serve the user. When the intensity of satellites is selected according to Lemma 2, the coverage probability remains constant (dashed lines) all over the Earth for any latitude.

Figure 5 illustrates the probability of coverage at different altitudes. For all propagation environments, the coverage probability increases to reach its maximum value as the altitude increases which is then followed by a decline due to the rise in the number of visible interfering satellites. The optimum altitude for $\phi_{\rm u} = 0°$ is slightly larger than $\phi_{\rm u} = 25°$, the reason being that the intensity of satellites, and consequently the number of interferers, is higher at upper latitudes. When the user's latitude is set to $\phi_{\rm u} = 65°$, which means that the user is located out of the constellation borders ($\phi_{\rm u} > \iota = 53°$), a larger altitude is crucial for the constellation so that the user can be served by a satellite within its visible range. As a result, for altitudes lower than about 400 km, no visible satellite is available to serve the user which results in zero coverage probability.

Several constellation design guidelines can be extracted from Figs. 4 and 5, e.g., regarding the orbital inclination and altitude. The inclination angle does not need to be necessarily

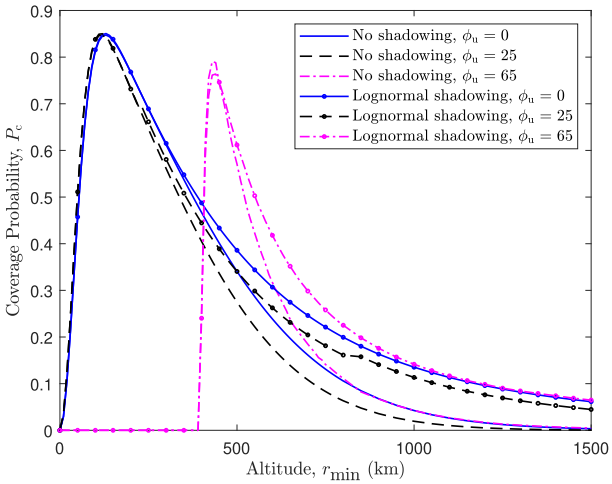

Fig. 5. Effect of altitude on coverage probability when $T = 5$ dB, $\phi_u = \{0°, 25°, 65°\}$, $\iota = 53°$, $m = 2$, and $\theta_{min} = 10°$. The expression given in Theorem 1 is used to plot this figure.

TABLE II
MINIMUM CONSTELLATION SIZE TO PROVIDE 90% COVERAGE PROBABILITY IN DIFFERENT CITIES

Cities	Helsinki ($\phi_u \approx 60°$ N)		Singapore ($\phi_u \approx 1°$ N)		Sydney ($\phi_u \approx 34°$ S)	
Altitude (km)	500	1500	500	1500	500	1500
Constellation size	380	560	230	300	165	210

greater than the maximum latitude of the intended service area and it may even result in better performance for some latitudes out of the constellation's borders as long as there are visible satellites to the user. On the other hand, increasing the inclination angle to avoid outage on higher latitudes necessitates more satellites to maintain the same density and, consequently, the same performance all over the service area. Similar compromise should be also considered for the altitude. Higher altitudes provide better chance of visibility for the users. However, the overall performance is degraded due to larger path attenuation at those altitudes.

Besides from the performance evaluation, the derivations in Theorems 1 and 2 can be utilized to determine different constellation parameters for a desired performance criterion. For instance, in Table II, we illustrate the minimum number of satellites needed to provide a coverage probability of at least 0.9 for a noise-limited LEO network in three different cities. The inclination angle is assumed to be 53°. As the user gets closer to the inclination limits (53°), fewer satellites can provide the desired performance. Moreover, a larger constellation size is required for higher altitudes in order to compensate for the greater path loss. For Helsinki, being on a higher latitude than the inclination angle, more satellites are required to achieve the same performance.

Figure 6 verifies the derivations for average data rate of a user at the latitude of 25°. As shown in the figure, the simulation results are perfectly in line with theoretical expressions

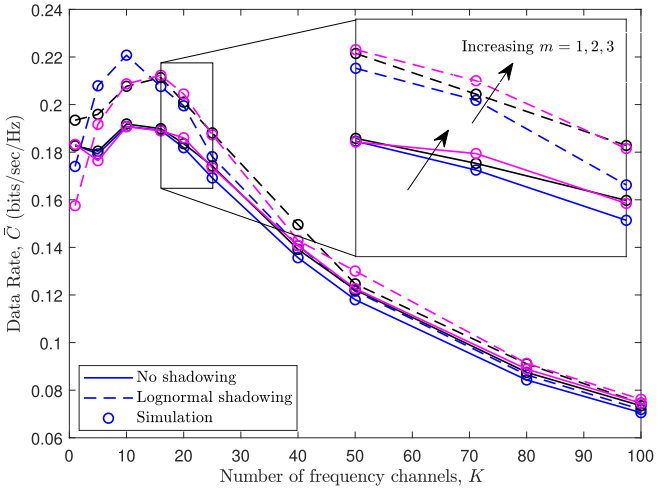

Fig. 6. Theorem 2 verification with simulations when $\phi_u = 25°$, $\iota = 53°$, $m \in \{1, 2, 3\}$, and $\theta_{min} = 10°$. The lines and the markers show the theoretical and simulation results, respectively.

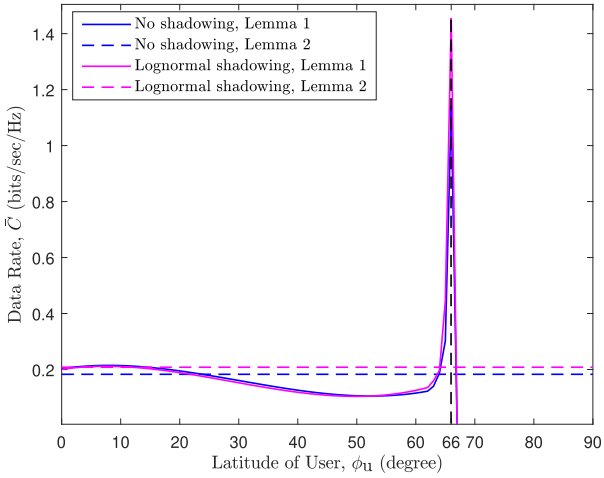

Fig. 7. Data rate on different users' latitudes, $K = 10$, $r_{min} = 500$ km, $\iota = 53°$, $m = 2$, and $\theta_{min} = 10°$. The expression given in Theorem 2 is used to plot this figure.

in Theorem 2. The disparate behaviour of the curves is caused by the two opposite effects of frequency reuse on the average achievable rate. As the number of frequency bands increases, the total number of interfering satellites on the same frequency band declines which results in an increase in the data rate. On the other hand, by increasing the number of frequency channels, the bandwidth shared among a group of satellites is reduced. An increase in the plot is observed at first as a result of the decrease in interference received power, followed by a drop which is due to comprising only $\frac{1}{K}$ of frequency band.

Figure 7, as a counterpart for Fig. 4, illustrates the variation of data rate over different latitudes when the intensity of Poisson point process is chosen to be according to Lemma 1 or, for comparison, Lemma 2. With intensity being as in Lemma 1, data rate varies over the different user's latitudes as shown in Fig. 7. For 53° inclined orbits, there is a minor decline in data rate which is followed by a sharp rise due to a decrease in the number of visible interfering satellites when the user leaves the inclination limits.

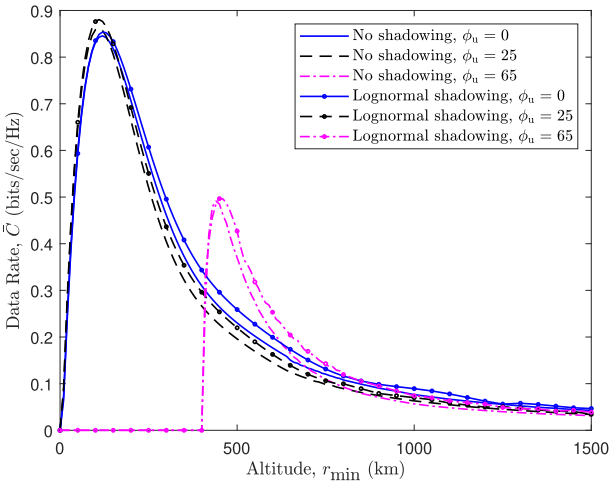

Fig. 8. Effect of altitude on data rate when $K = 10$, $\phi_u = \{0°, 25°, 65°\}$, $\iota = 53°$, $m = 2$, and $\theta_{\min} = 10°$. The expression given in Theorem 2 is used to plot this figure.

The effect of altitude on data rate is depicted in Fig. 8 for $K = 10$. Similar to Fig. 5, from the minimum altitude at which the user is able to visit at least one satellite, the data rate increases rapidly until reaches a maximum point. After the maximum point, the data rate decreases more slowly due to the increase in the number of interfering satellites as well as satellites being at a farther distance from the user. The altitude which maximizes the data rate varies with the user's latitude and, obviously, it has similar value which results in the maximum coverage probability.

V. Conclusion

In this paper, a generic approach to obtain the analytical performance of a massive low Earth orbit network was presented by modeling the satellites' locations as a nonhomogeneous Poisson point process and utilizing the tools from stochastic geometry. The density of the nonhomogeneous Poisson point process is derived from the actual geometry of the constellation which enables us to take into account the non-uniform distribution of satellites across different latitudes. Our next step was to apply this model to derive analytical expressions for the coverage probability and average data rate of an arbitrarily located user in terms of the distribution of fading and shadowing as well as the Laplace function of interference. From the numerical results, we concluded that, depending on the shadowing parameters, the effect of shadowing on the network performance is ambivalent. Furthermore, we showed how the analytical results allow one to find — without involved orbital simulations — optimum values for altitude, the number of orthogonal frequency channels, and user's latitude which result in the largest coverage and/or throughput, given the constellation parameters.

Appendix A
Proof of Lemma 3

For a NPPP, the CDF of R_0 can be written as

$$F_{R_0}(r_0) = 1 - \mathbb{P}(R_0 > r_0) = 1 - \mathbb{P}(\mathcal{N} = 0), \quad (26)$$

where $\mathbb{P}(\mathcal{N} = 0)$ is the void probability of PPP in $\mathcal{A}(r_0)$ that can be obtained from (7) by setting $n = 0$. According to (7), by integrating from the intensity over the spherical cap above the user, we have

$$\begin{aligned} F_{R_0}(r_0) &= 1 - \exp\left(-\int_{\max(\phi_u-\phi_0,-\iota)}^{\min(\phi_u+\phi_0,\iota)} \beta(\phi_s)\delta(\phi_s)\left(r_{\min}+r_\oplus\right)^2 \cos(\phi_s) d\phi_s\right) \\ &\overset{(a)}{=} 1 - \exp\left(-2\left(r_{\min}+r_\oplus\right)^2 \int_{\max(\phi_u-\phi_0,-\iota)}^{\min(\phi_u+\phi_0,\iota)} \delta(\phi_s)\cos(\phi_s) \right. \\ &\qquad \left. \times \cos^{-1}\left(\frac{\cos(\phi_0)}{\cos(\phi_s-\phi_u)}\right) d\phi_s\right), \end{aligned} \quad (27)$$

where $\beta(\phi_s)$ is the longitude range inside the spherical cap above the user at latitude ϕ_s. Equality (a) follows from substitution of $\beta(\phi_s)$ using the basic geometry. Taking the derivative of (27) with respect to r_0 completes the proof of Lemma 3. Note that for $\phi_0 \leq |\phi_u| - \iota$ the CDF given in (27) is zero since the spherical cap formed by polar angle ϕ_0 above the latitude ϕ_u is much farther from the constellation's borders to contain any satellite.

Appendix B
Proof of Theorem 1

To obtain the expression given (16), let us begin with the definition of coverage probability:

$$\begin{aligned} P_c(T) &= \mathbb{E}_{R_0}\left[\mathbb{P}\left(\mathrm{SINR} > T | R_0\right)\right] \\ &= \int_{r_{\min}}^{r_{\max}} \mathbb{P}\left(\mathrm{SINR} > T | R_0 = r_0\right) f_{R_0}(r_0)\, dr_0 \\ &= \int_{r_{\min}}^{r_{\max}} \mathbb{P}\left(\frac{p_t G_t(r_0) H_0 \mathcal{X}_0 r_0^{-\alpha}}{I+\sigma^2} > T\right) f_{R_0}(r_0)\, dr_0 \\ &= \int_{r_{\min}}^{r_{\max}} \mathbb{E}_I\left[\mathbb{P}\left(H_0\mathcal{X}_0 > \frac{T r_0^\alpha \left(I+\sigma^2\right)}{p_t G_t(r_0)}\right) \middle| I > 0\right] \\ &\qquad \times f_{R_0}(r_0)\, dr_0. \end{aligned} \quad (28)$$

Since satellites with elevation angles smaller than $\theta_{\min}$ are not visible to the user, the integral has an upper limit. Then

$$\begin{aligned} P_c(T) &\overset{(a)}{=} \int_{r_{\min}}^{r_{\max}} \mathbb{E}_I\left[\int_0^\infty f_{\mathcal{X}_0}(x_0)\left(1 - F_{H_0}\left(\frac{T r_0^\alpha \left(I+\sigma^2\right)}{p_t G_t(r_0) x_0}\right)\right)\right] \\ &\qquad \times f_{R_0}(r_0)\, dx_0 dr_0 \\ &\overset{(b)}{=} \int_{r_{\min}}^{r_{\max}} \mathbb{E}_I\left[\int_0^\infty f_{\mathcal{X}_0}(x_0)\left(\frac{\Gamma\left(m_0, m_0 \frac{T r_0^\alpha \left(I+\sigma^2\right)}{p_t G_t(r_0) x_0}\right)}{\Gamma(m_0)}\right)\right] \\ &\qquad \times f_{R_0}(r_0)\, dx_0 dr_0 \\ &\overset{(c)}{=} \int_{r_{\min}}^{r_{\max}} \int_0^\infty f_{\mathcal{X}_0}(x_0) f_{R_0}(r_0)\, e^{-\frac{m_0 T r_0^\alpha \sigma^2}{p_t G_t(r_0) x_0}} \mathbb{E}_I\left[e^{-\frac{m_0 T r_0^\alpha I}{p_t G_t(r_0) x_0}}\right. \end{aligned}$$

$$\sum_{k=0}^{m_0-1}\frac{\sum_{l=0}^{k}\binom{k}{l}\left(m_0\frac{Tr_0^{\alpha}\sigma^2}{p_tG_t(r_0)x_0}\right)^{l}\left(m_0\frac{Tr_0^{\alpha}I}{p_tG_t(r_0)x_0}\right)^{k-l}}{k!}\Bigg]dx_0dr_0$$
$$=\int_{r_{\min}}^{r_{\max}}\int_0^{\infty}f_{\mathcal{X}_0}(x_0)f_{R_0}(r_0)\Bigg[e^{-s\sigma^2}$$
$$\sum_{k=0}^{m_0-1}\frac{\sum_{l=0}^{k}\binom{k}{l}\left(s\sigma^2\right)^{l}(-s)^{k-l}\frac{\partial^{k-l}}{\partial s^{k-l}}\mathcal{L}_I(s)}{k!}\Bigg]_{s=\frac{m_0Tr_0^{\alpha}}{p_tG_t(r_0)x_0}}dx_0dr_0. \tag{29}$$

The substitution in (a) follows from the product distribution of two independent random variables, (b) follows from the distribution of gamma random variable H_0 (being the square of the Nakagami random variable), and (c) is calculated by applying the incomplete gamma function for integer values of m_0 to (b).

Appendix C
Proof of Theorem 2

Most of the steps in derivation of the data rate expression, given in Theorem 2, are similar to those given in Appendix B. According to the definition of the average data rate given in (17), we have

$$\begin{aligned}\bar{C}&=\mathbb{E}_{I,H_0,\mathcal{X}_0,R_0}\left[\log_2\left(1+\mathrm{SINR}\right)\right]\\&=\int_{r_{\min}}^{r_{\max}}\mathbb{E}_{I,H_0,\mathcal{X}_0}\left[\log_2\left(1+\frac{p_tG_t(r_0)H_0\mathcal{X}_0r_0^{-\alpha}}{\sigma^2+I}\right)\right]f_{R_0}(r_0)\,dr_0\\&\overset{(a)}{=}\int_{r_{\min}}^{r_{\max}}\int_0^{\infty}\mathbb{E}_{I,H_0,\mathcal{X}_0}\left[\mathbb{P}\left(\log_2\left(1+\frac{p_tG_t(r_0)H_0\mathcal{X}_0r_0^{-\alpha}}{\sigma^2+I}\right)>t\right)\right]\\&\qquad\times f_{R_0}(r_0)\,dtdr_0\\&=\int_{r_{\min}}^{r_{\max}}\int_0^{\infty}\mathbb{E}_{I,H_0,\mathcal{X}_0}\left[\mathbb{P}\left(H_0\mathcal{X}_0>\frac{r_0^{\alpha}\left(\sigma^2+I\right)}{p_tG_t(r_0)}\left(2^t-1\right)\right)\right]\\&\qquad\times f_{R_0}(r_0)\,dtdr_0\end{aligned} \tag{30}$$

where (a) follows form the fact that for a positive random variable X, $\mathbb{E}[X]=\int_{t>0}\mathbb{P}(X>t)\,dt$. Thus, we have

$$\begin{aligned}\bar{C}&\overset{(a)}{=}\int_{r_{\min}}^{r_{\max}}\int_0^{\infty}\mathbb{E}_I\Bigg[\int_0^{\infty}f_{\mathcal{X}_0}(x_0)\\&\quad\times\left(1-F_{H_0}\left(\frac{r_0^{\alpha}\left(I+\sigma^2\right)\left(2^t-1\right)}{p_tG_t(r_0)x_0}\right)\right)dx_0\Bigg]f_{R_0}(r_0)\,dt\;dr_0\\&\overset{(b)}{=}\int_{r_{\min}}^{r_{\max}}\int_0^{\infty}\mathbb{E}_I\Bigg[\int_0^{\infty}f_{\mathcal{X}_0}(x_0)\\&\quad\times\left(\frac{\Gamma\left(m_0,m_0\frac{r_0^{\alpha}\left(I+\sigma^2\right)\left(2^t-1\right)}{p_tG_t(r_0)x_0}\right)}{\Gamma(m_0)}\right)dx_0\Bigg]f_{R_0}(r_0)\,dtdr_0\\&\overset{(c)}{=}\int_{r_{\min}}^{r_{\max}}\int_0^{\infty}\int_0^{\infty}f_{\mathcal{X}_0}(x_0)f_{R_0}(r_0)e^{-\frac{m_0\left(2^t-1\right)r_0^{\alpha}\sigma^2}{p_tG_t(r_0)x_0}}\\&\quad\times\mathbb{E}_I\left[e^{-\frac{m_0\left(2^t-1\right)r_0^{\alpha}I}{p_tG_t(r_0)x_0}}\right.\end{aligned}$$
$$\sum_{k=0}^{m_0-1}\frac{\sum_{l=0}^{k}\binom{k}{l}\left(\frac{m_0\left(2^t-1\right)r_0^{\alpha}\sigma^2}{p_tG_t(r_0)x_0}\right)^{l}\left(\frac{m_0\left(2^t-1\right)r_0^{\alpha}I}{p_tG_t(r_0)x_0}\right)^{k-l}}{k!}\Bigg]dtdx_0dr_0$$
$$=\int_{r_{\min}}^{r_{\max}}\int_0^{\infty}\int_0^{\infty}f_{\mathcal{X}_0}(x_0)f_{R_0}(r_0)\Bigg[e^{-s\sigma^2}$$
$$\sum_{k=0}^{m_0-1}\frac{\sum_{l=0}^{k}\binom{k}{l}\left(s\sigma^2\right)^{l}(-s)^{k-l}\frac{\partial^{k-l}}{\partial s^{k-l}}\mathcal{L}_I(s)}{k!}\Bigg]_{s=\frac{m_0\left(2^t-1\right)r_0^{\alpha}}{p_tG_t(r_0)x_0}}dtdx_0dr_0. \tag{31}$$

Similar to the proof of Theorem 1, (a) follows from the product distribution of two independent random variables, (b) follows from the gamma distribution of serving channel gain H_0, and (c) is calculated by applying the incomplete gamma function for integer values of m_0 to (b).

Appendix D
Proof of Lemma 5

In this appendix, we derive the expression for Laplace function of interference assuming arbitrary distributions for fading and shadowing. Let us start with the definition of Laplace function for random variable I which is

$$\begin{aligned}\mathcal{L}_I(s)&\triangleq\mathbb{E}_I\left[e^{-sI}\right]\\&=\mathbb{E}_{\mathcal{N},R_n,\mathcal{X}_n,H_n}\left[\exp\left(-s\sum_{n\in\xi\setminus\{s\}}p_tG_t(R_n)H_n\mathcal{X}_nR_n^{-\alpha}\right)\right]\\&=\mathbb{E}_{\mathcal{N},R_n,\mathcal{X}_n,H_n}\left[\prod_{n\in\xi\setminus\{s\}}\exp\left(-sp_tG_t(R_n)H_n\mathcal{X}_nR_n^{-\alpha}\right)\right].\end{aligned} \tag{32}$$

Due to i.i.d. distribution of H_n and $\mathcal{X}_n$ as well as their independence from $\mathcal{N}$ and R_n, we have

$$\begin{aligned}&\mathcal{L}_I(s)\\&=\mathbb{E}_{\mathcal{N},R_n}\left[\prod_{n\in\xi\setminus\{s\}}\mathbb{E}_{\mathcal{X}_n,H_n}\left[\exp\left(-sp_tG_t(R_n)H_n\mathcal{X}_nR_n^{-\alpha}\right)\right]\right]\end{aligned} \tag{33}$$

$$\begin{aligned}&\overset{(a)}{=}\mathbb{E}_{\mathcal{N}}\Bigg[\prod_{n\in\xi\setminus\{s\}}\int_{r_0}^{r_{\max}}\mathbb{E}_{\mathcal{X}_n,H_n}\left[\exp\left(-sp_tG_t(r_n)H_n\mathcal{X}_nr_n^{-\alpha}\right)\right]\\&\qquad\times f_{R_n|R_0}(r_n|r_0)dr_n\Bigg],\end{aligned} \tag{34}$$

where (a) is obtained by taking the expectation over the random variable R_n conditioned on R_0. Then

$$\begin{aligned}\mathcal{L}_I(s)&\overset{(b)}{=}\sum_{n=0}^{\infty}P_n\left(\mathcal{A}(r_{\max})-\mathcal{A}(r_0)\right)\\&\quad\times\Bigg(\int_{r_0}^{r_{\max}}\mathbb{E}_{\mathcal{X}_n,H_n}\left[\exp\left(-sp_tG_t(r_n)H_n\mathcal{X}_nr_n^{-\alpha}\right)\right]\\&\qquad\times f_{R_n|R_0}(r_n|r_0)dr_n\Bigg)^n\end{aligned}$$

$$\stackrel{(c)}{=} \sum_{n=0}^{\infty} P_n \left(\mathcal{A}\left(r_{\max}\right) - \mathcal{A}\left(r_0\right) \right) \times \left(\int_{r_0}^{r_{\max}} \int_0^{\infty} \mathcal{L}_{H_n}\left(s p_{\mathrm{t}} G_{\mathrm{t}}(r_n) x_n r_n^{-\alpha} \right) \times f_{\mathcal{X}_n}(x_n) f_{R_n|R_0}(r_n|r_0) dx_0 dr_n \right)^n, \quad (35)$$

where $\mathcal{A}\left(r_{\max}\right) - \mathcal{A}\left(r_0\right)$ indicates the region above the user where satellites which are more distanced from the user than the serving satellite exist, (b) is obtained by taking the average over the Poisson random variable $\mathcal{N}$, and applying the law of total expectation on independent random variables H_n and $\mathcal{X}_n$ results in (c).

REFERENCES

[1] M. Giordani and M. Zorzi, "Non-terrestrial networks in the 6G era: Challenges and opportunities," *IEEE Netw.*, vol. 35, no. 2, pp. 244–251, Mar. 2021.

[2] Z. Jia, M. Sheng, J. Li, D. Zhou, and Z. Han, "Joint HAP access and LEO satellite backhaul in 6G: Matching game-based approaches," *IEEE J. Sel. Areas Commun.*, vol. 39, no. 4, pp. 1147–1159, Apr. 2021.

[3] M. Giordani and M. Zorzi, "Satellite communication at millimeter waves: A key enabler of the 6G era," in *Proc. Int. Conf. Comput., Netw. Commun. (ICNC)*, Feb. 2020, pp. 383–388.

[4] M. Giordani *et al.*, "Toward 6G networks: Use cases and technologies," *IEEE Commun. Mag.*, vol. 58, no. 3, pp. 55–61, Dec. 2020.

[5] J. L. Grubb, "The traveler's dream come true," *IEEE Commun. Mag.*, vol. 29, no. 11, pp. 48–51, Nov. 1991.

[6] A. Mokhtar and M. Azizoglu, "On the downlink throughput of a broadband LEO satellite network with hopping beams," *IEEE Commun. Lett.*, vol. 4, no. 12, pp. 390–393, Dec. 2000.

[7] F. Vatalaro, G. E. Corazza, C. Caini, and C. Ferrarelli, "Analysis of LEO, MEO, and GEO global mobile satellite systems in the presence of interference and fading," *IEEE J. Sel. Areas Commun.*, vol. 13, no. 2, pp. 291–300, Feb. 1995.

[8] A. Ganz, Y. Gong, and B. Li, "Performance study of low Earth-orbit satellite systems," *IEEE Trans. Commun.*, vol. 42, no. 234, pp. 1866–1871, Feb. 1994.

[9] I. Ali, N. Al-Dhahir, and J. E. Hershey, "Predicting the visibility of LEO satellites," *IEEE Trans. Aerosp. Electron. Syst.*, vol. 35, no. 4, pp. 1183–1190, Oct. 1999.

[10] Y. Seyedi and S. M. Safavi, "On the analysis of random coverage time in mobile LEO satellite communications," *IEEE Commun. Lett.*, vol. 16, no. 5, pp. 612–615, May 2012.

[11] Z. Qu, G. Zhang, H. Cao, and J. Xie, "Leo satellite constellation for Internet of Things," *IEEE Access*, vol. 5, pp. 18391–18401, 2017.

[12] M. Haenggi, *Stochastic Geometry for Wireless Networks*. Cambridge, U.K.: Cambridge Univ. Press, 2012.

[13] B. Błaszczyszyn, M. Haenggi, P. Keeler, and S. Mukherjee, *Stochastic Geometry Analysis of Cellular Networks*. Cambridge, U.K.: Cambridge Univ. Press, 2018.

[14] M. Haenggi, J. G. Andrews, F. Baccelli, O. Dousse, and M. Franceschetti, "Stochastic geometry and random graphs for the analysis and design of wireless networks," *IEEE J. Sel. Areas Commun.*, vol. 27, no. 7, pp. 1029–1046, Aug. 2009.

[15] H. Elsawy, E. Hossain, and M. Haenggi, "Stochastic geometry for modeling, analysis, and design of multi-tier and cognitive cellular wireless networks: A survey," *IEEE Commun. Surveys Tuts.*, vol. 15, no. 3, pp. 996–1019, Jun. 2013.

[16] J. G. Andrews, F. Baccelli, and R. K. Ganti, "A tractable approach to coverage and rate in cellular networks," *IEEE Trans. Commun.*, vol. 59, no. 11, pp. 3122–3134, Nov. 2011.

[17] H. S. Dhillon, R. K. Ganti, F. Baccelli, and J. G. Andrews, "Modeling and analysis of K-tier downlink heterogeneous cellular networks," *IEEE J. Sel. Areas Commun.*, vol. 30, no. 3, pp. 550–560, Apr. 2012.

[18] D. Cao, S. Zhou, and Z. Niu, "Optimal combination of base station densities for energy-efficient two-tier heterogeneous cellular networks," *IEEE Trans. Wireless Commun.*, vol. 12, no. 9, pp. 4350–4362, Sep. 2013.

[19] H. S. Dhillon, T. D. Novlan, and J. G. Andrews, "Coverage probability of uplink cellular networks," in *Proc. IEEE Global Commun. Conf. (GLOBECOM)*, Dec. 2012, pp. 2179–2184.

[20] M. Afshang and H. S. Dhillon, "Fundamentals of modeling finite wireless networks using binomial point process," *IEEE Trans. Wireless Commun.*, vol. 16, no. 5, pp. 3355–3370, May 2017.

[21] Z. Pan and Q. Zhu, "Modeling and analysis of coverage in 3-D cellular networks," *IEEE Commun. Lett.*, vol. 19, no. 5, pp. 831–834, May 2015.

[22] V. V. Chetlur and H. S. Dhillon, "Downlink coverage analysis for a finite 3-D wireless network of unmanned aerial vehicles," *IEEE Trans. Commun.*, vol. 65, no. 10, pp. 4543–4558, Jul. 2017.

[23] S. Srinivasa and M. Haenggi, "Distance distributions in finite uniformly random networks: Theory and applications," *IEEE Trans. Veh. Technol.*, vol. 59, no. 2, pp. 940–949, Feb. 2010.

[24] J. Guo, S. Durrani, and X. Zhou, "Outage probability in arbitrarily-shaped finite wireless networks," *IEEE Trans. Commun.*, vol. 62, no. 2, pp. 699–712, Feb. 2014.

[25] Z. Khalid and S. Durrani, "Distance distributions in regular polygons," *IEEE Trans. Veh. Technol.*, vol. 62, no. 5, pp. 2363–2368, Jun. 2013.

[26] X. Wang, H. Zhang, Y. Tian, and V. C. M. Leung, "Modeling and analysis of aerial base station-assisted cellular networks in finite areas under LoS and NLoS propagation," *IEEE Trans. Wireless Commun.*, vol. 17, no. 10, pp. 6985–7000, Oct. 2018.

[27] J. Guo, S. Durrani, and X. Zhou, "Performance analysis of arbitrarily-shaped underlay cognitive networks: Effects of secondary user activity protocols," *IEEE Trans. Commun.*, vol. 63, no. 2, pp. 376–389, Feb. 2015.

[28] T. A. Khan and M. Afshang, "A stochastic geometry approach to Doppler characterization in a LEO satellite network," in *Proc. IEEE Int. Conf. Commun. (ICC)*, Jun. 2020, pp. 1–6.

[29] J. Hu, G. Li, D. Bian, L. Gou, and C. Wang, "Optimal power control for cognitive LEO constellation with terrestrial networks," *IEEE Commun. Lett.*, vol. 24, no. 3, pp. 622–625, Mar. 2020.

[30] J. Zhang, B. Evans, M. A. Imran, X. Zhang, and W. Wang, "Performance analysis of C/U split hybrid satellite terrestrial network for 5G systems," in *Proc. IEEE 20th Int. Workshop Comput. Aided Modeling Design Commun. Links Netw. (CAMAD)*, Sep. 2015, pp. 97–102.

[31] A. J. Roumeliotis, C. I. Kourogiorgas, and A. D. Panagopoulos, "Optimal dynamic capacity allocation for high throughput satellite communications systems," *IEEE Wireless Commun. Lett.*, vol. 8, no. 2, pp. 596–599, Apr. 2019.

[32] A. K. Dwivedi, S. Praneeth Chokkarapu, S. Chaudhari, and N. Varshney, "Performance analysis of novel direct access schemes for LEO satellites based IoT network," in *Proc. IEEE 31st Annu. Int. Symp. Pers., Indoor Mobile Radio Commun.*, Aug. 2020, pp. 1–6.

[33] N. Okati, T. Riihonen, D. Korpi, I. Angervuori, and R. Wichman, "Downlink coverage and rate analysis of low Earth orbit satellite constellations using stochastic geometry," *IEEE Trans. Commun.*, vol. 68, no. 8, pp. 5120–5134, Aug. 2020.

[34] N. Okati and T. Riihonen, "Stochastic analysis of satellite broadband by mega-constellations with inclined LEOs," in *Proc. IEEE 31st Annu. Int. Symp. Pers., Indoor Mobile Radio Commun.*, Aug. 2020, pp. 1–6.

[35] N. Okati and T. Riihonen, "Modeling and analysis of LEO mega-constellations as nonhomogeneous Poisson point processes," in *Proc. IEEE 93rd Veh. Technol. Conf. (VTC-Spring)*, Apr. 2021, pp. 1–5.

[36] A. Al-Hourani, "An analytic approach for modeling the coverage performance of dense satellite networks," *IEEE Wireless Commun. Lett.*, vol. 10, no. 4, pp. 897–901, Apr. 2021.

[37] A. Al-Hourani, "Optimal satellite constellation altitude for maximal coverage," *IEEE Wireless Commun. Lett.*, vol. 10, no. 7, pp. 1444–1448, Jul. 2021.

[38] A. Talgat, M. A. Kishk, and M.-S. Alouini, "Nearest neighbor and contact distance distribution for binomial point process on spherical surfaces," *IEEE Commun. Lett.*, vol. 24, no. 12, pp. 2659–2663, Dec. 2020.

[39] A. Talgat, M. A. Kishk, and M.-S. Alouini, "Stochastic geometry-based analysis of LEO satellite communication systems," *IEEE Commun. Lett.*, vol. 25, no. 8, pp. 2458–2462, Aug. 2021.

[40] A. Yastrebova *et al.*, "Theoretical and simulation-based analysis of terrestrial interference to LEO satellite uplinks," in *Proc. GLOBECOM IEEE Global Commun. Conf.*, Dec. 2020, pp. 1–6.
[41] Z. Khalid and S. Durrani, "Connectivity of three dimensional wireless sensor networks using geometrical probability," in *Proc. Austral. Commun. Theory Workshop (AusCTW)*, Jan. 2013, pp. 47–51.
[42] *Attenuation by Atmospheric Gases and Related Effects*, document Recommendation ITU-R, 676–12, Aug. 2019.
[43] I. D. Portillo, B. G. Cameron, and E. F. Crawley, "A technical comparison of three low earth orbit satellite constellation systems to provide global broadband," *Acta Astronautica*, vol. 159, pp. 123–135, Jun. 2019. [Online]. Available: https://www.sciencedirect.com/science/article/pii/S0094576518320368
[44] I. S. Gradshteyn and I. M. Ryzhik, *Table of Integrals, Series, and Products*. New York, NY, USA: Academic, 2014.

Niloofar Okati received the B.Sc. degree in electrical engineering from the Shiraz University of Technology, Iran, in 2013, and the M.Sc. degree in communications engineering from the Iran University of Science and Technology (IUST), Iran, in 2016. She is currently pursuing the Ph.D. degree with the Faculty of Information Technology and Communication Sciences, Tampere University, Finland. Her research interests include stochastic geometry, wireless communication, and satellite networks. She was one of the 200 young researchers in mathematics and computer science selected worldwide to participate in the Seventh Heidelberg Laureate Forum (HLF) in 2019.

Taneli Riihonen (Member, IEEE) received the D.Sc. degree (Hons.) in electrical engineering from Aalto University, Helsinki, Finland, in August 2014. He is currently an Assistant Professor (tenure track) with the Faculty of Information Technology and Communication Sciences, Tampere University, Finland. He held various research positions at the Aalto University School of Electrical Engineering from September 2005 to December 2017. He was a Visiting Associate Research Scientist and an Adjunct Assistant Professor with Columbia University, New York, USA, from November 2014 to December 2015. His research activity is focused on physical-layer OFDM (A), multiantenna, relaying, and full-duplex wireless techniques with current interest in the evolution of beyond 5G systems. He received the Finnish Technical Sector's Award for the Best Doctoral Dissertation in 2014 and the EURASIP Best Ph.D. Thesis Award in 2017. He has been nominated 11 times as an exemplary/top reviewer of various IEEE journals and is serving as an Editor for IEEE WIRELESS COMMUNICATIONS LETTERS since May 2017. He has served as an Editor for IEEE COMMUNICATIONS LETTERS from October 2014 to January 2019.